Multiscale Finite Element Modeling of Arc Dynamics in a DC Plasma Torch

Juan Pablo Trelles,[1] Emil Pfender,[1] and Joachim Heberlein[1]

The dynamics of the electric arc inside a direct current non-transferred arc plasma torch are simulated using a three-dimensional, transient, equilibrium model. The fluid and electromagnetic equations are solved numerically in a fully coupled approach by a multiscale finite element method. Simulations of a torch operating with argon and argon-hydrogen under different operating conditions are presented. The model is able to predict the operation of the torch in steady and takeover modes without any further assumption on the reattachment process except for the use of an artificially high electrical conductivity near the electrodes, needed because of the equilibrium assumption. The results obtained indicate that the reattachment process in these operating modes may be driven by the movement of the arc rather than by a breakdown-like process. It is also found that, for a torch operating in these modes and using straight gas injection, the arc will tend to re-attach to the opposite side of its original attachment. This phenomenon seems to be produced by a net angular momentum on the arc due to the balance between magnetic and fluid drag forces.

KEY WORDS: Thermal plasma; torch; modeling; arc dynamics; finite elements; multiscale.

NOTATION

$\vec{A}$	magnetic vector potential [T-m]
$\mathbf{A}$	advective Jacobian
$\mathbf{A_0}$	transformation Jacobian from conservative to primitive variables
$\vec{B}$	magnetic field [T]
C_p	specific heat at constant pressure [J/kg-K]
e	elementary charge [C]
$\vec{E}$	electric field [V/m]
h	enthalpy [J/kg] and convective heat transfer coefficient [W/m^2-K]
I	total current [A]
$\vec{j}$	current density [A/m^2]
k_B	Boltzmann constant [J/K]
$\mathbf{K}$	diffusivity matrix
$\mathbf{K}_{DCO}$	discontinuity-capturing-operator diffusivity matrix
n	normal to the boundary
$\mathbf{N}$	basis or interpolation function
p	pressure [Pa]
$\mathbf{q_0}$, $\mathbf{q_1}$	linearizations of specified diffusive fluxes
Q	volumetric flow rate [lpm]
r	radial coordinate [m]
$\mathcal{R}$	total residual of the conservation equations
R	radius [m]
S	boundary of the computational domain
$\mathbf{S_0}$, $\mathbf{S_1}$	reactive terms (i.e. linearizations of a general source term **S**)

[1] Department of Mechanical Engineering, University of Minnesota, Minneapolis, MN 55455, USA

t	time [s]
T	temperature [K]
$\vec{u}$	velocity [m/s]
U	average velocity [m/s]
V	computational domain
$\mathbf{X}$	vector of spatial coordinates
$\mathbf{Y}$	vector of unknowns
x, y, z	main coordinate axes [m]
$\hat{x}$, $\hat{y}$, $\hat{z}$	unit vectors of the main axes

Greek Symbols

α	Polar coordinated angle [rad]
$\vec{\vec{\delta}}$	identity tensor
ε_r	net emission coefficient [W/m^3-sr]
ϕ	electric potential [V]
κ	thermal conductivity [W/m-K]
μ	dynamic viscosity [kg/m-s]
μ_0	permeability of free space [Wb/A-m]
ρ	density [kg/m^3]
σ	electrical conductivity [1/Ω-m]
$\vec{\tau}$	stress tensor [Pa]
$\boldsymbol{\tau}_{SGS}$	matrix of time scales
θ	average inclination angle of the inlet flow with respect to the torch axis [rad]

Subscripts, Superscripts

a, c	anode, cathode
in	inlet conditions
w	cooling water

1. INTRODUCTION

Plasma spraying, one of the most widely used industrial applications based on thermal plasmas, is commonly employed to provide coatings for protection of materials against wear, erosion, corrosion, and thermal loads. Despite its versatility, the limited reproducibility of the processes is a major limitation for its wider application. A major factor for this limited reproducibility is the lack of understanding and control of the dynamics of the arc inside the spraying torch and, the effect of erosion of the anode on the forcing of the plasma jet.

Figure 1 shows a schematic representation of the flow inside a direct current (DC), non-transferred arc plasma torch, as typically used in plasma spraying. After the working gas enters the torch, it is heated by the arc formed between a nozzle-shaped anode and a cylindrical cathode, forming a plasma, which is ejected as a jet[(1)]. It can be observed that, despite the axisymmetry of the geometry and boundary conditions (i.e. inflow velocity profile, constant potential at the anode surface), the flow is inherently three-dimensional. Furthermore, any movement of the arc (i.e. movement of the anode attachment) will significantly affect the outflow from the torch, forcing the jet.

The dynamics of the arc are a result of the balance between the drag force caused by the interaction of the incoming gas flow over the arc and the electromagnetic (or Lorentz) force caused by the local curvature of the arc[(2)]. The length of the arc is proportional to the variation of the magnitude of the voltage fluctuations. Three different modes of operation of the torch have

been identified according to these voltage fluctuations (see Fig. 2). These are, in order of decreasing current or increasing flow rate[2, 3, 4, 5, 6, 7]:

- *Steady mode*, characterized by an almost fixed position of the anode attachment and correspondingly negligible voltage fluctuations; this mode is not desirable because it causes the rapid erosion of the anode.
- *Takeover mode*, characterized by a periodic or quasi-periodic movement of the arc and voltage fluctuations; this operating mode is currently the most desirable for the operation of plasma spraying torches, as it allows an adequate distribution of the heat load over the anode, and the well defined fluctuations of the arc allow a more predictable forcing of the jet.
- *Restrike mode*, characterized by a highly unstable, relatively unpredictable movement of the arc and quasi-chaotic, large amplitude, voltage fluctuations. This mode dramatically forces the jet, enhancing cold flow entrainment and turbulence development, limiting the reproducibility of the spraying process.

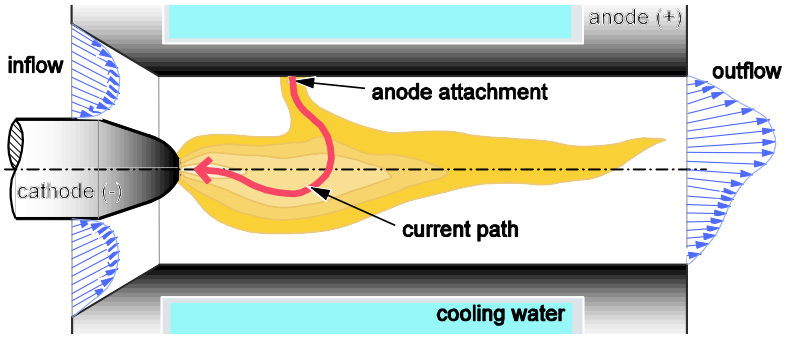

Fig. 1. Idealized representation of the flow inside a DC non-transferred arc plasma torch.

A possibly ideal movement of the arc will be quasi-periodic, with high frequency and small amplitude, hence distributing uniformly the thermal load over the anode while forcing the jet homogenously. To obtain design/control strategies to achieve such a movement, a better understanding of the processes driving the dynamics of the arc is required.

Due to the strongly radiating nature of the arc, added to its confinement inside the torch, the direct observation of the complete dynamics of the arc inside the torch is extremely difficult, if not impossible; hence the motivation to use adequate numerical models (i.e. models capable of predicting the different modes of operation of the torch) to enhance our understanding of the arc dynamics.

The modeling of the arc in DC plasma torches is very challenging because the flow is inherently three-dimensional, unsteady, highly nonlinear, with large gradients, requiring a wide range of time and spatial scales for its description. In addition, chemical and thermodynamic non-equilibrium effects have to be considered, especially near the boundaries of the plasma. Hence a minimum requirement for the description of the arc dynamics requires a three-dimensional and transient model. Even though non-equilibrium effects are important, especially near the electrodes and in regions where the arc interacts with the cold flow, due to the added complexity and computational cost, only models based on the Local Thermodynamic Equilibrium (LTE) assumption have been presented so far.

One of the first three-dimensional, but steady-state, simulation of the arc inside a DC torch was performed by Li *et al* initially in Ref. 8 by relying on the occurrence of numerical instabilities in the iterative process to drive the solution to develop a fixed attachment, and then in Ref. 9 by using Steenbeck's minimum principle (also known as the principle of minimum entropy production applied to thermal plasmas) to fix the position of the anode attachment. Gonzales *et al*[10], using the commercial software FLUENT, also performed steady-state simulations of the arc. In their initial work they assumed a position of the attachment by arbitrarily imposing a region

with high temperature and high electrical conductivity; however, they were not able to obtain a convergent solution with this approach. Imposing a constant high electrical conductivity over the anode surface allowed them to obtain a steady-state solution. Klinger *et al*[11] performed steady-state simulations of the arc by arbitrarily specifying the position of the attachment by means of imposing a current density profile over the anode and neglecting the magnetic effects. It is important to mention that any steady-state solution of an inherently transient phenomenon (i.e. torch operating in takeover mode) is artificial and is an indication of the unsuitability of the mathematical (i.e. specified boundary conditions) and/or numerical model employed (i.e. using a method with excessive numerical diffusion helps to obtain convergence, but will damp the unsteady characteristics of the problem).

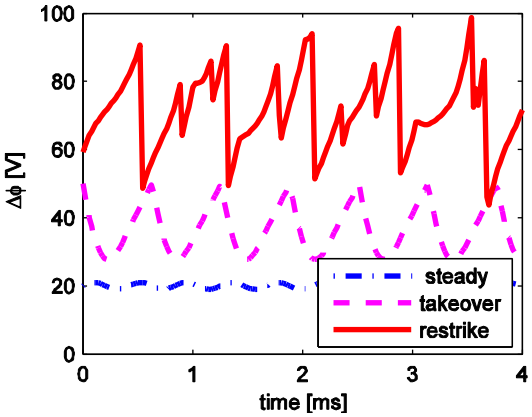

Fig. 2. Schematic representation of the voltage signal for different operating modes in DC non-transferred arc plasma torches.

A transient simulation of the movement of an arc driven by a rotating magnetic field was performed by Park *et al*[12]; their model was able to predict the azimuthal movement of the arc inside the torch due to the action of the imposed magnetic field, but not the axial motion that arises from the imbalance between drag and magnetic forces. Baudry *et al*[13, 14, 15], using the code ESTET, and through the use of non-standard boundary conditions, developed a model able to capture the displacement of the anode spot as caused by the interaction of the cold flow with the plasma, and described the reattachment process by specifying a maximum electric field, acting as a control parameter. After the electric field of the arc reaches this maximum value, an artificial hot column, simulating a new attachment, is established at a predefined position upstream. As the simulation proceeds, the arc equilibrates to this new attachment, simulating the reattachment process. By controlling the value of the specified maximum electric field, the reattachment frequency can be controlled. More recently, Colombo and Ghedini[16], also relying on the commercial software FLUENT, simulated the plasma flow in a DC torch with the same geometry used in Ref. 8 and 9 but for a low current and flow rate, without any further assumption on the reattachment process except for the use of an artificially high electrical conductivity, as it is done here.

Due to the inherent multiscale nature of the plasma flow inside the torch, turbulence models are desirable and have been included in some of the former simulations, i.e. k-ε Reynolds-Averaged Navier-Stokes (RANS) models have been used in Refs. 8, 9 and 12, and even a Smagorinsky sub-grid scale model, as commonly used in Large Eddy Simulations (LES), has been used in Ref. 16. There are severe limitations, which have not been addressed so far, with the use of standard turbulence models for the modeling of thermal plasmas, especially in regions where the electromagnetic effects are important (as is the case for the flow inside the torch). In particular the k-ε model does not include a turbulence production term[17] due to the Lorentz force which enhances vorticity production, especially near the plasma-cold flow interface[18], in

addition the assumption of isotropy in the Smagorinsky model is not valid due to the Lorentz force, and any attempt to perform a LES needs to consider the adequate resolution of the grid-resolved scales of the flow.

In this research, in order to handle the multiscale nature of the arc dynamics, we have developed an implicit, robust, high order, numerical code which solves the fluid and electromagnetic equations in a fully coupled manner and is based on the variational multiscale method, specifically, on the algebraic Sub-Grid Scale Finite Element Method (SGS-FEM)[19, 20, 21, 22, 23], which implicitly accounts for the multiscale nature of the flow by modeling the characteristics of the flow unable to be solved with practical numerical resolutions. This method has been extensively developed and validated and seems promising for the description of complex multiscale phenomena, such as thermal plasma flows. Furthermore, as most methods used for the simulation of thermal plasmas have relied on SIMPLE-like algorithms (except for the work of Klinger *et al*[11] and Kaddani *et al*[24] of a free-burning arc), the use of a different numerical method tests the suitability of former numerical models, as a true solution should be independent of the numerical method employed. Moreover, this is the first time that a variational multiscale finite element method is applied to thermal plasma simulation. We expect that the inherent advantages of modern finite element methods will make them very attractive for plasma phenomena simulation, as shown by Georghiou *et al*[25] in their review of finite element simulations of non-thermal plasmas.

The goal of this research is to obtain an adequate model of the dynamics of the arc inside DC plasma torches and to develop a qualitative description of the factors driving the re-attachment process. Section 2 presents the mathematical model, which is based on the LTE assumption and includes compressibility effects (as in Ref. 11), the computational domain which corresponds to the same geometry used in Refs. 13, 14 and 15, and boundary conditions, which are handled in a similar form as used in Ref. 16. Section 3 presents the numerical model based on the SGS-FEM and a brief description of the developed solver. Section 4 presents results of simulations of the torch operating with argon and argon-hydrogen (75-25% vol) under realistic operating conditions (as used in Ref. 8 and 9 and Refs. 13, 14, 15), including a detailed description of the reattachment process and the voltage spectra obtained. Conclusions and future directions to improve simulations of the arc dynamics are presented in section 5.

2. MATHEMATICAL MODEL

2.1. Model Assumptions

It is assumed: (1) The continuum assumption is valid and the plasma can be considered as a compressible, perfect gas in Local Thermodynamic Equilibrium (LTE), hence characterized by a single temperature for all its species (atoms, ions, electrons, molecules); (2) the quasi-neutrality condition holds; (3) the plasma is optically thin; (4) Hall currents, gravitational effects, and viscous dissipation are considered negligible; (5) when mixtures of gases are used, they are assumed to remain perfectly mixed at their chemical equilibrium composition (a model with a detailed treatment of species diffusion, as the one used by Murphy[26], will be able to simulate demixing which alters the heat transfer to the anode).

2.2. Governing Equations

The fluid equations governing a thermal plasma under the above assumptions are the same as for a compressible fluid with the addition of several source terms, and are given by the equations of conservation of mass, momentum, and energy. The electromagnetic equations are given by Maxwell's equations which, according to our assumptions, can be expressed in a reduced form in terms of the electric potential and magnetic vector potential as the current conservation equation and a form of the magnetic induction equation. The set of equations used is:

$$\frac{\partial \rho}{\partial t} + \nabla \cdot \rho \vec{u} = 0 \qquad (1)$$

$$\rho\left(\frac{\partial \vec{u}}{\partial t}+\vec{u}\cdot\nabla\vec{u}\right)=-\nabla p-\nabla\cdot\vec{\tau}+\vec{j}\times\vec{B} \tag{2}$$

$$\rho C_p\left(\frac{\partial T}{\partial t}+\vec{u}\cdot\nabla T\right)=\nabla\cdot\left(\kappa\nabla T\right)+\vec{j}\cdot\left(\vec{E}+\vec{u}\times\vec{B}\right)-4\pi\varepsilon_r+\frac{5}{2}\frac{k_B}{e}\vec{j}\cdot\nabla T+\frac{Dp}{Dt} \tag{3}$$

$$\nabla\cdot\left(\sigma\nabla\phi\right)=0 \tag{4}$$

$$\nabla^2\vec{A}=-\mu_0\vec{j} \tag{5}$$

where the term $\vec{j}\times\vec{B}$ represents the Lorentz force; $\vec{j}\cdot\vec{E}$ the Joule heating term; the term $4\pi\varepsilon_r$ represents the volumetric radiation losses; the term proportional to $\vec{j}\cdot\nabla T$ represents the diffusion of electron enthalpy; the last term in equation (3) represents the pressure work (equal to zero in constant density flows), with D/Dt as the substantial derivative.

These equations are complemented with appropriate relations for the calculation of thermodynamic and transport properties (based on the chemical and kinetic equilibrium assumption, and obtained here from a computer code developed in our laboratory[27]) and the following additional relations:

$$\vec{\tau}=-\mu\left(\nabla\vec{u}+\nabla\vec{u}^{\,T}-\frac{2}{3}\nabla\cdot\vec{u}\,\vec{\delta}\right) \tag{6}$$

$$\nabla\times\vec{A}=\vec{B},\quad \vec{E}=-\nabla\phi-\frac{\partial\vec{A}}{\partial t}\quad\text{and}\quad \vec{j}=\sigma\vec{E} \tag{7}$$

We solve this system of equations in terms of the primitive variables p, $\vec{u}$, T, ϕ, $\vec{A}$ instead of the conservation variables ρ, $\rho\vec{u}$, ρh, ϕ, $\vec{A}$ because they are better for attaining numerical convergence. For example, in flows where compressibility effects may become important in some regions and negligible in others, i.e. in a region of the flow where compressibility effects are negligible, density does not change (hence its gradient is zero) whereas pressure and its gradient are always well defined in every region of the flow (see Ref. 20). Then, we express the mass conservation equation in terms of primitive variables as follows:

$$\rho\nabla\cdot\vec{u}+\left(\frac{\partial\rho}{\partial p}\right)\left(\frac{\partial p}{\partial t}+\vec{u}\cdot\nabla p\right)+\left(\frac{\partial\rho}{\partial T}\right)\left(\frac{\partial T}{\partial t}+\vec{u}\cdot\nabla T\right)=0. \tag{8}$$

The second term in equation (8) represents the compressibility effects due to pressure variations ($\partial\rho/\partial p$ is equal to the inverse of the sound speed squared), whereas the third term is due to temperature variations. It is a common approach in simulations of thermal plasmas to neglect the second term in equation (8) as well as the pressure work term in equation (3), considering the flow as density-varying quasi-incompressible. For an argon plasma with a velocity of 1000 m/s and at a temperature of 10000 K (conditions that are easily met inside a DC torch), the local sound speed is almost 2000 m/s and hence the local Mach number is ~0.5; therefore compressibility effects may not be negligible. The common practice stated above is likely to be due to the fact that most software used for simulating plasma flows is based on incompressible flow solvers modified to include the electromagnetic effects (exceptions are the works by Kaddani *et al*[24] and Klinger *et al*[11]).

2.3. Computational Domain and Boundary Conditions

The geometry of the problem corresponds to part of the F4-MB Sulzer-Metco plasma spraying torch. This geometry is the same studied in Refs. 13, 14 and 15, but the computational domain has been extended upstream to include the effect of the incoming flow on the arc. The domain is discretized using trilinear hexahedral finite elements (8 nodes per element). Figure 3 presents the computational domain, the discretization mesh, and the division of the boundary in different *sides* to define boundary conditions; whereas table 1 presents the boundary conditions applied.

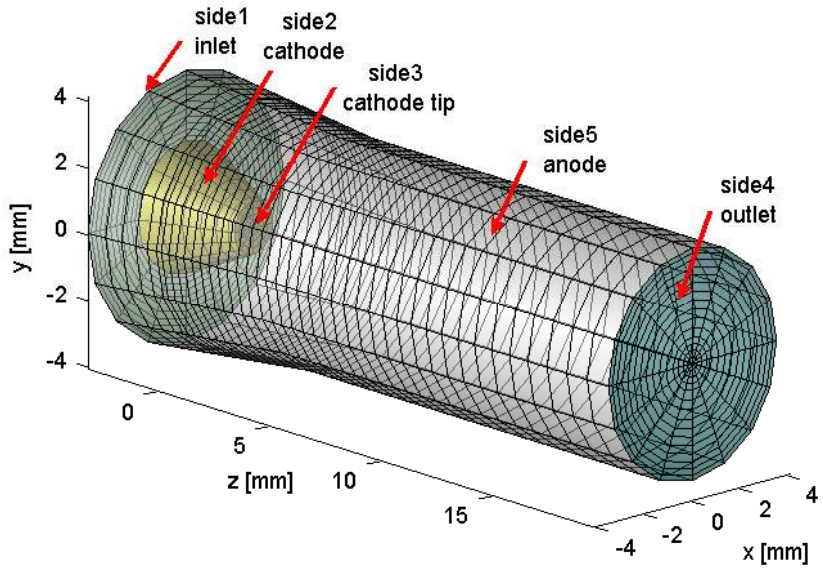

Fig. 3. Computational domain, mesh and division of the boundary.

Table 1. Boundary conditions.

	p	$\vec{u}$	T	ϕ	$\vec{A}$
side1 inlet	$p = p_0$	$\vec{u} = \vec{u}_{in}$	$T = T_{in}$	$\frac{\partial \phi}{\partial n} = 0$	$A_i = 0$
side2 cathode	$\frac{\partial p}{\partial n} = 0$	$u_i = 0$	$T = T_{cath}$	$\frac{\partial \phi}{\partial n} = 0$	$\frac{\partial A_i}{\partial n} = 0$
side3 cathode tip	$\frac{\partial p}{\partial n} = 0$	$u_i = 0$	$T = T_{cath}$	$-\sigma \frac{\partial \phi}{\partial n} = j_{cathtip}$	$\frac{\partial A_i}{\partial n} = 0$
side4 outlet	$\frac{\partial p}{\partial n} = 0$	$\frac{\partial u_i}{\partial n} = 0$	$\frac{\partial T}{\partial n} = 0$	$\frac{\partial \phi}{\partial n} = 0$	$A_i = 0$
side5 anode	$\frac{\partial p}{\partial n} = 0$	$u_i = 0$	$-\kappa \frac{\partial T}{\partial n} = h_w (T - T_w)$	$\phi = 0$	$\frac{\partial A_i}{\partial n} = 0$

In table 1, $i = x$, y, or z. The non-slip assumption is imposed over all solid boundaries. At the inlet, a reference pressure of $p_0 = 0$ kPa and a temperature $T_{in} = 1000$ K are imposed (hence a negative pressure is obtained at the outlet), as well as a quasi-parabolic velocity profile (fully developed laminar flow through an annulus), from which the components of velocity are obtained according to:

$$U_1 = 2U_{in}\left(1 - \left(\frac{r}{R_a}\right)^2 + \left(1 - k^2\right)\frac{\ln\left(r/R_a\right)}{\ln\left(1/k\right)}\right) \Bigg/ \left(1 + k^2 - \frac{\left(1 - k^2\right)}{\ln\left(1/k\right)}\right) \tag{9}$$

$$\vec{u}_x = -U_1 \sin(\theta)\cos(\alpha)\hat{x}, \quad \vec{u}_y = -U_1 \sin(\theta)\sin(\alpha)\hat{y}, \quad \vec{u}_z = U_1 \cos(\theta)\hat{z} \tag{10}$$

$$k = \frac{R_c}{R_a} \quad \text{and} \quad U_{in} = \frac{Q_{in}}{\pi R_a^2 (1 - k^2)} \tag{11}$$

To better study the natural dynamics of the arc, no swirl component has been included (differently from Refs. 13, 14, 15 and Ref. 16).

Even though the imposition of a reference pressure at the outlet is the most common condition in simulations of internal flows (and is actually required for the well-posedness of steady-state SIMPLE-like solvers), we found it to be too reflective, i.e. it caused an arc reattachment further upstream than when imposing the pressure at the inlet. An alternative used in Refs. 13, 14, 15 is to impose locally either a static or a stagnation pressure at the outlet, depending on the direction of the flow, and hence force the flow to leave the domain. Other alternatives, more elaborate and not so standard, consist of the imposition of a zero second derivative at the outlet (which is usually numerically unstable) and the use of non-reflecting boundary conditions based on the method of characteristics (which are commonly employed in aeroacoustics). The approach that we consider the best consists of extending the domain (as done in Ref. 16) and imposing a fixed reference pressure at the outlet surface. We have not followed this approach in the present work due to its computational cost but we plan to use it in future simulations.

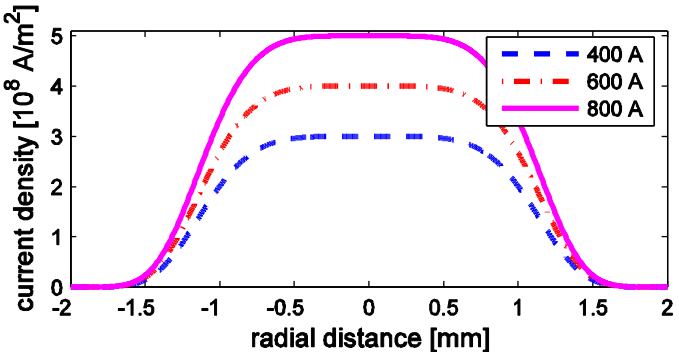

Fig. 4. Current density profiles defined over cathode tip.

At the cathode surface, a Gaussian-like temperature profile $T_{cath}(z)$, varying from 1000 at the inlet to 3600 K at the tip is imposed, as well as a current density profile $j_{cathtip}$ of the form:

$$j_{cathtip} = j_0 \exp\left(-(r/r_c)^{n_c}\right) \tag{12}$$

Values of $j_0 = 3 \cdot 10^8$, $4 \cdot 10^8$ and $5 \cdot 10^8$ A/m^2 are chosen for total currents of $I = 400$, 600 and 800 A respectively, $n_c = 5$, and the value of r_c is chosen to ensure that the integration of this profile over the cathode tip area is equal to the imposed total current (i.e. for $I = 600$ A, $r_c \approx 0.75$ mm). This form of $j_{cathtip}$ was chosen to try to mimic approximately the current density profiles reported by Zhou and Heberlein[28]. Figure 4 shows the form of the employed profiles for different currents. Even though these profiles may not represent properly the widening that occurs as the total current is increased, they were limited by the size and shape of the cathode tip diameter of ~1.6 mm. Due to the almost direct relation between current density and the Lorentz force, it is expected that the velocity profile in front of the cathode resembles in some extent the form of the current density profile over the cathode. Hence, the use of a sharper $j_{cathtip}$ profile (i.e. the use of a larger j_0) will produce a cathode jet with a higher maximum velocity at the center and a more rapid decaying towards its fringes. The effect of varying $j_{cathtip}$ for a given current has not been studied in the present paper but will be considered in future publications.

At the anode surface, a convective boundary condition is imposed as done in Ref. 15 with a convective heat transfer coefficient h_w equal to $1\cdot10^5$ W/m^2-K and a reference cooling water temperature equal to 500 K. A better alternative would be to impose this condition at some region within the anode (i.e. include part of the anode in the computational domain), as done in Refs. 8 and 9. However our assumption of a negligible temperature drop in the anode wall may be justified due to the high thermal conductivity of copper.

The boundary conditions imposed on the components of the magnetic vector potential are standard[10, 12, 13, 14, 15] and, although not mathematically rigorous, do not violate Ampere's law $\nabla \times \vec{B} = \mu_0 \vec{j}$.

Due to the thermal equilibrium assumption, the value of the electron temperature (which determines the electrical conductivity) is equal to that of the heavy particles, which is low near the anode (i.e. less than 3000 K). Hence the equilibrium electrical conductivity is extremely low ($<1\cdot10^{-4}$ 1/Ω-m), limiting the continuity of the electrical current through the boundaries. Common approaches to alleviate this situation are the use of an artificially high electrical conductivity or a sheath model near the electrodes. In this research, an artificially high electrical conductivity equal to $8\cdot10^3$ 1/Ω-m, which corresponds to an electron temperature of ~15000 K for pure argon, is imposed on a layer of 0.1 mm of thickness right in front of the anode. The high electrical conductivity assumption is justified by the fact that the electron temperature is expected to be high near the arc attachment as the electrons are accelerated towards the anode.

3. NUMERICAL MODEL

3.1. Matrix Form of the Thermal Plasma Equations

The system of fluid and electromagnetic equations expressed by equations (1) to (5) can be written in compact form as a system of transient-advective-diffusive-reactive equations in terms of the vector of unknowns $\mathbf{Y} = \left[p \quad \vec{u} \quad T \quad \phi \quad \vec{A} \right]^T$ according to:

$$\mathcal{R}(\mathbf{Y}) = \underbrace{\mathbf{A_0}\,\partial\mathbf{Y}/\partial t}_{\text{transient}} + \underbrace{\left(\mathbf{A}^T\nabla\right)\mathbf{Y}}_{\text{advective}} - \underbrace{\nabla^T\left(\mathbf{K}\nabla\mathbf{Y}\right)}_{\text{diffusive}} - \underbrace{\mathbf{S_1Y} - \mathbf{S_0}}_{\text{reactive}} = \mathbf{0} \quad \text{over} \quad V \tag{13}$$

$$\mathbf{Y} = \mathbf{Y}_{fix} \qquad \text{over } S_1 \tag{14}$$

$$\mathbf{K}\frac{\partial\mathbf{Y}}{\partial n} + \mathbf{q_0} + \mathbf{q_1Y} = 0 \qquad \text{over } S_2 \tag{15}$$

All the terms in equation (13) are matrices of adequate sizes and are, in general, functions of t, $\mathbf{X}$, $\mathbf{Y}$, $\partial\mathbf{Y}/\partial t$, $\nabla\mathbf{Y}$. The reader is referred to Ref. 21 for the exact form of these matrices in the context of compressible flows. Equation (14) represents the specification of fixed-value (Dirichlet) boundary conditions over part of the boundary of V specified by S_1, and equation (15) represents the specification of diffusive fluxes (Neumann or Robin) boundary conditions over the rest of the boundary (specified by S_2).

3.2. Sub-Grid Scale Finite Element Method

There are several problems associated with the solution of general advection-diffusion-reaction equations. These problems are common to almost all numerical methods used for the solution of PDEs (i.e. finite differences, volumes, elements, spectral methods), and are associated with the disparity among time and spatial scales. These problems translate into spurious, non-physical oscillations of the solution field if an insufficiently fine computational mesh is used. The approach of Direct Numerical Simulation (DNS), which is mostly associated with the modeling of turbulent flows, looks for solving all scales of the flow, hence using extremely fine meshes, and extremely small time steps.

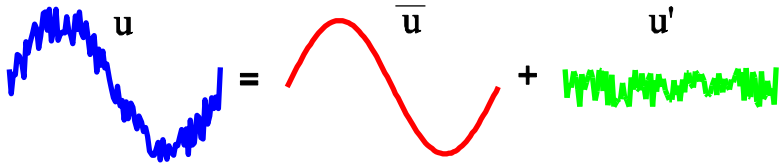

Fig. 5. Division of the solution of a given variable *u* into its large (grid resolved) and small (sub-grid, modeled) scale components.

Variational multiscale methods solve this problem by separating the solution of a given field into a large scale component (solved by the method) plus a small or sub-grid scale component (modeled), as depicted in Fig. 5. This formulation is consistent as the "sub-grid modeling term" becomes negligible as the discretization mesh becomes finer[23]. Variational multiscale methods seem promising for the modeling of complex flows with a wide range of scales (i.e. large Reynolds numbers), in complex domains, as found in industrial applications, for which DNSs may not be feasible in the near future; they even have been successful on simulating the problem of bypass turbulent transition[32]. The interested reader is referred to Ref. 23 for a recent review of variational multiscale methods.

The algebraic sub-grid scale finite element method (SGS-FEM) is one of the simplest formulations of the variational multiscale method, in which the large and fine scales are approximated with the same computational grid (see i.e. Ref. 22). The SGS-FEM model of the system given by equations (13) to (15) is expressed as:

$$\underbrace{\int_V \mathbf{N}^T\left(\mathbf{A_0}\frac{\partial \mathbf{Y}}{\partial t}+\left(\mathbf{A}^T\cdot\nabla\right)\mathbf{Y}-\mathbf{S_1Y}-\mathbf{S_0}\right)dV+\int_V(\nabla\mathbf{N})^T(\mathbf{K}\nabla\mathbf{Y})dV+\oint_{s_2}\mathbf{N}^T(\mathbf{q_0}+\mathbf{q_1Y})dS+}_{\text{Galerkin}}$$

$$\underbrace{\int_V \mathcal{P}(\mathbf{N})^T\boldsymbol{\tau}_{SGS}\mathcal{R}(\mathbf{Y})dV}_{\text{sub-grid scale}}+\underbrace{\int_V(\nabla\mathbf{N})^T(\mathbf{K}_{DCO}\nabla\mathbf{Y})dV}_{\text{discontinuity capturing}}=0 \qquad (16)$$

where the basis, or interpolation function $\mathbf{N} = \mathbf{N}(x, y, z)$ is typical of any finite element (if $\mathbf{N} = 1$, we obtain a finite volume method); the Galerkin term represents the part solved by the mesh (large scale); the sub-grid scale term represents the modeling of the small scales, with $\mathcal{P}$ the negative of the adjoint of the differential operator applied to $\mathbf{Y}$ in equation (13), and $\boldsymbol{\tau}_{SGS}$ is the model parameter. The discontinuity capturing operator is added due to the fact that the method is not monotonically preserving (i.e. a high order method can present oscillations near sharp discontinuities, like shock waves), and $\mathbf{K}_{DCO}$ is negligible when the solution is smooth. The $\boldsymbol{\tau}_{SGS}$ and $\mathbf{K}_{DCO}$ used in this research are based on the ones developed in Ref. 21; more details about these terms can be found in Refs. 29 and 30.

3.3. HTPLFLOW code

The SGS-FEM applied to nonlinear transient advective-diffusive-reactive systems has been implemented in the code HTPLFLOW (*High Temperature and PLasma FLOW solver*) developed in our laboratory. The code is capable to solve an arbitrary number of coupled equations in any number of spatial dimensions on unstructured grids in a fully implicit manner using the generalized-α time stepping method developed in Ref. 30 and automatic time step control. The required solution of a non-linear system of equations at each time interval is performed by a line-search algorithm with an inexact Newton method and a direct sparse solver. The code has been

validated with 0, 1, 2 and 3D problems, including incompressible flow benchmark problems, axisymmetric simulations of DC plasma torches, and a three-dimensional simulation of an arc in cross-flow. Figure 6 shows results of the driven cavity flow problem, a standard benchmark problem in computational fluid dynamics. This problem consists on a square cavity in which a constant tangential velocity U_0 in the x direction is imposed to its upper boundary while the other boundaries are kept at rest. The developed flow has specific characteristics (i.e. size, number, and position of vortices) according to the Reynolds number based on the imposed velocity and the size of the cavity. As can be seen in Fig. 6, even for a high Reynolds number, the results obtained with a 121x121 mesh of bilinear elements compare well with those obtained by Ghia *et al*[33] using a finer mesh, indicating the higher order approximation obtained by the SGS-FEM.

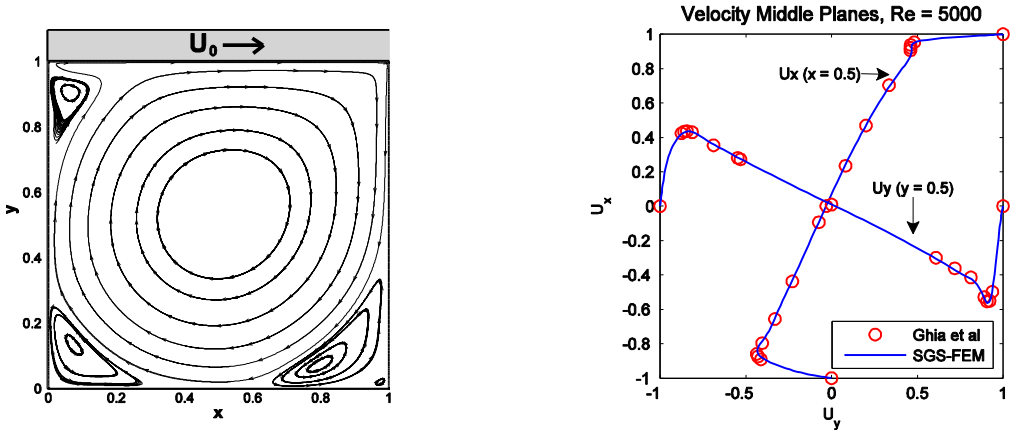

Fig. 6. Driven cavity flow problem at Reynolds number equal to 5000: (left) problem definition and streamlines, (right) velocity components through middle planes.

4. MODELING RESULTS AND DISCUSSION

4.1. Torch Operating with Argon and Argon-Hydrogen

Table 2 presents the conditions of the different cases simulated. Figure 7 shows different views of the temperature distribution throughout the torch for case number 4 after 210 time steps. The effects of the initial conditions have been dissipated after the first 120 time steps (typically, the effects of initial conditions are dissipated between the 70 and 130 initial time steps). Time steps between 0.1 and 1.0 μs were used, with the smaller time steps required near the formation of a new attachment. Figure 7 clearly shows the three dimensional nature of the plasma inside the torch, as well as its strong interaction with the incoming gas. Also, the plots of the temperature distribution at different axial cross sections indicates that the asymmetries caused by the arc attachment are mitigated as the plasma flows downstream; near the torch exit, the maximum temperature is located near the torch axis. The temperature distribution in the anode region shows approximately the extent of the anode attachment, located in the bottom part of the torch. Even though the attachment may seem diffuse, it is certainly much more constricted than the one obtained in the simulation using pure argon. It is expected that the use of better boundary conditions, i.e. the inclusion of part of the anode region in the calculation domain, and the use of a finer mesh will allow a better description of the attachment. However, only the use of a non-equilibrium model would provide realistic results of the attachment region.

Table 2. Operating conditions for simulated cases.

case	Current [A]	Flow Rate [slpm]	Gas
1	400	60	Ar-H_2 (75-25)
2	600	60	Ar-H_2 (75-25)
3	800	60	Ar-H_2 (75-25)
4	800	90	Ar-H_2 (75-25)

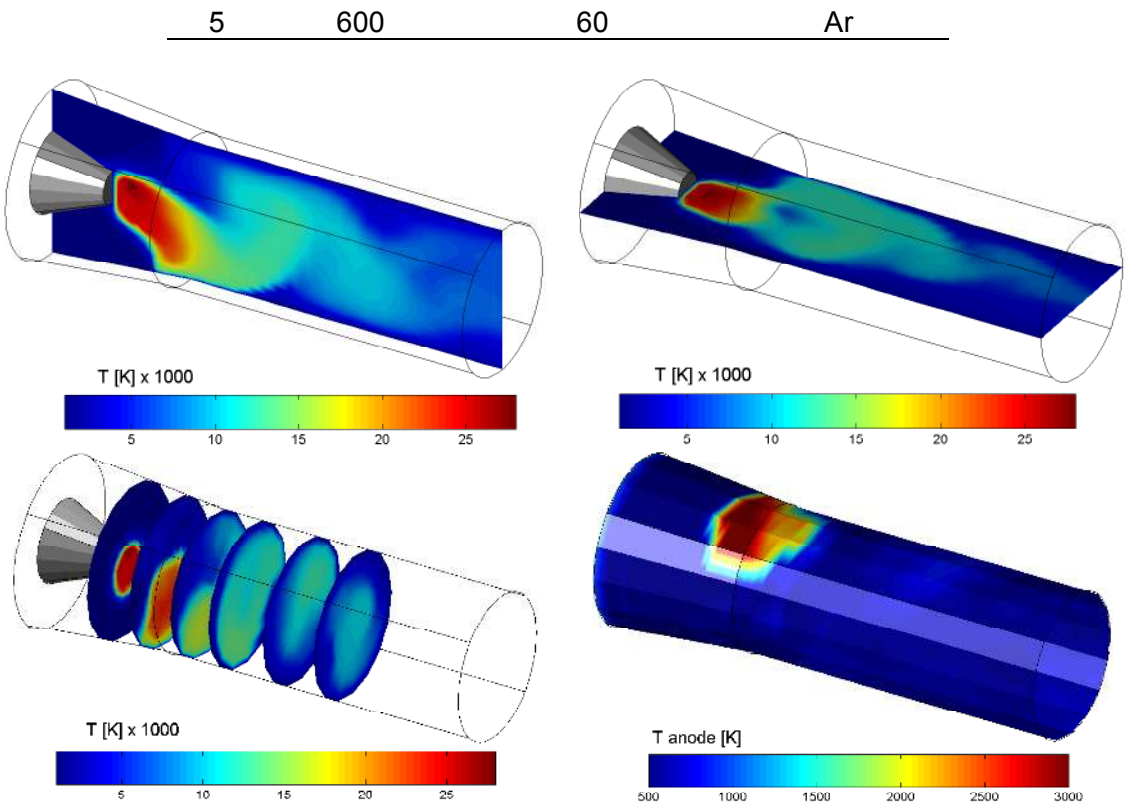

Fig. 7. Temperature distribution for case 4: Through vertical plane (top left), horizontal plane (top right), different cross sections (bottom left); and over the anode (bottom right), the *y* axis has been inverted.

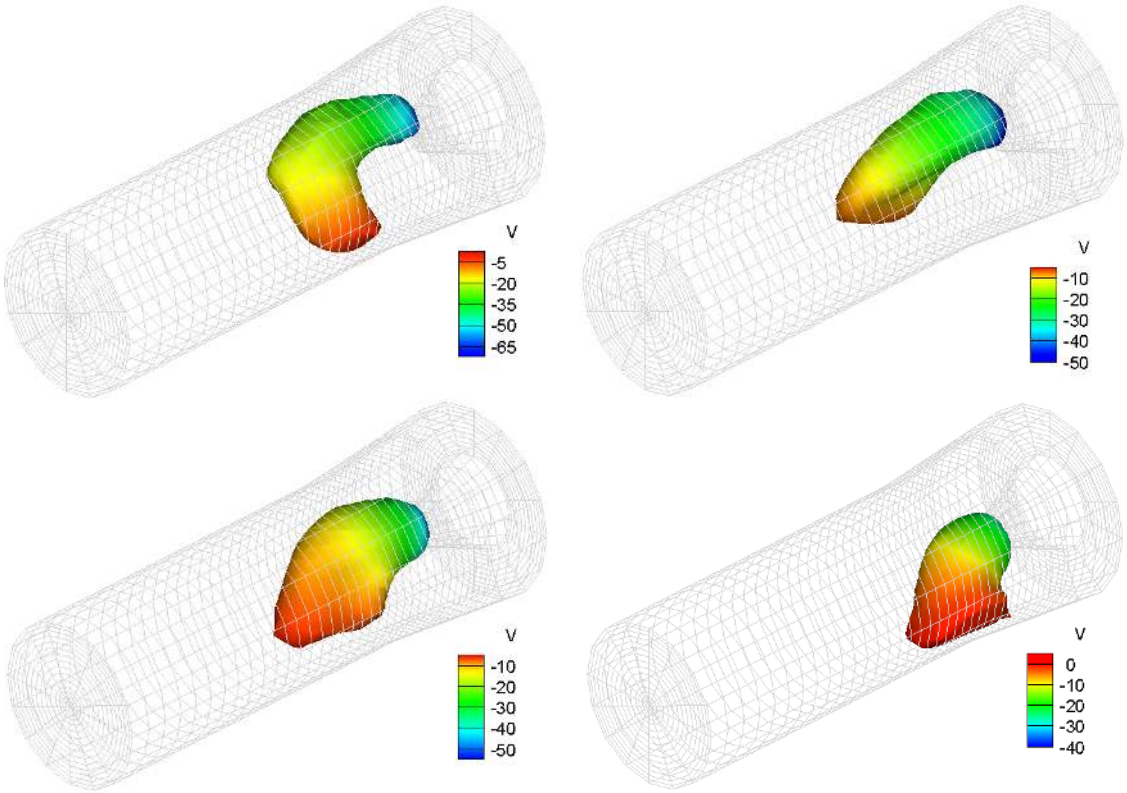

Fig. 8. Voltage distribution over the temperature isosurface of 14000 K for: case 1 (top left), case 2 (top right), case 3 (bottom left), and case 5 (bottom right).

Figure 8 shows the distribution of electric potential over the temperature isosurface of 14000 K, which approximately indicates the shape of the arc, for different cases. It can be observed that, as the total current is increased (from case 1 to 3), the arc becomes more robust, is deflected less by the flow, and the total voltage drop is reduced. The plot for case 5 indicates that the arc is more diffuse when operating with argon, which translates into a smaller voltage drop, and less acceleration of the flow.

4.2. Arc Reattachment Process

Figure 9 shows a time sequence of the reattachment process for case 1. As no breakdown model is used, a reattachment is formed whenever the arc gets "close enough" to the anode, the required proximity being a function of the thickness of the region in front of the anode specified with an artificially high electrical conductivity (~0.1 mm). The use of a sheath model may not improve the prediction of the reattachment process because the proximity distance will still be a function of the pre-specified sheath thickness. It could be argued that the results depend on the thickness of this high electrical conductivity layer, and indeed they do somewhat. Simulations using a thickness of ~0.2 mm produced higher reattachment frequencies, whereas results with a thickness of ~0.05 mm reproduced basically the same results as here, although it was harder to obtain convergence due to sharper gradients near the anode. Hence, physical insight needs to be considered when defining this thickness.

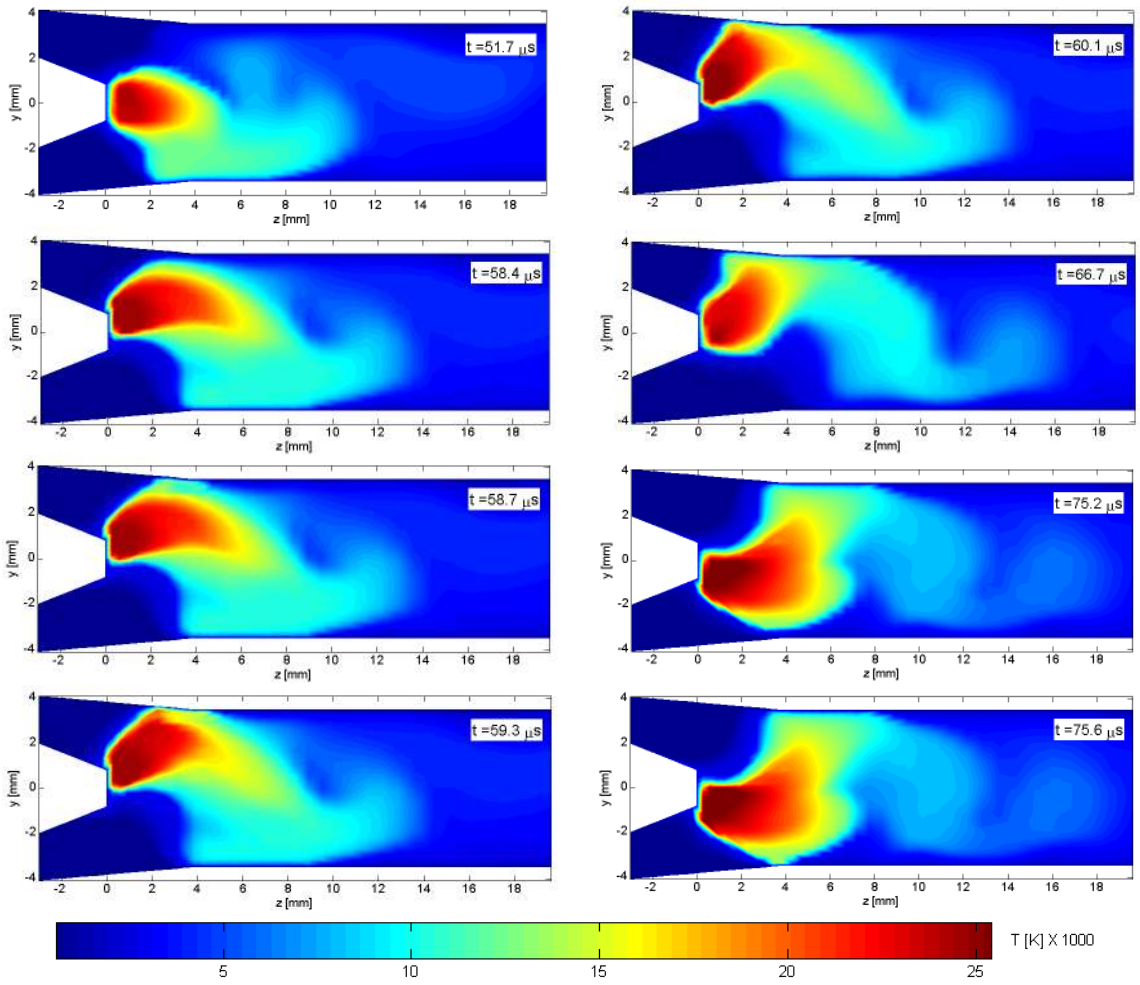

Fig. 9. Formation of a new attachment for case 2. Temperature distribution through vertical plane.

Despite the marked difference between the reattachment frequency obtained and that measured (i.e. by a factor of ~2), as explained in the next section, the current approach to model the reattachment process may be adequate for a reasonable description of the dynamics of the arc. It is also expected that the suitability of this model to simulate the dynamics of the arc will diminish as the arc is driven towards the restrike mode of operation, as non-equilibrium effects (i.e. UV excitation) may lead to a streamer-like breakdown process upstream of the existing attachment, forming a new one, as observed experimentally in Ref. 2.

One finding of the performed simulations is that, if straight injection is used, the arc tends to re-attach to the opposite side of its original attachment. This type of movement may be due to three factors: the effect of the Lorentz force acting along the arc, the variation of momentum caused by the anode jet (produced by the Lorentz force acting near the attachment), and the solid-body-like moment caused by the interaction of the gas flow on the arc. The Lorentz force acts wherever there is a local curvature of the arc; due to the varying shape of the arc, the Lorentz force generates an angular momentum which can either be positive (favoring) or negative (opposing) the formation of an attachment at the opposite side, as depicted in Fig. 10a and 10b. The anode jet is produced by the localized distribution of current density, which causes magnetic pumping (high magnetic pressure), and hence ejects the flow perpendicularly away from the anode surface, pushing the arc to a reattachment at the opposite side. Finally, as seen in Fig. 10d, the net drag force acting on the arc causes a net angular momentum that favors the formation of a new attachment at the opposite side of the original one.

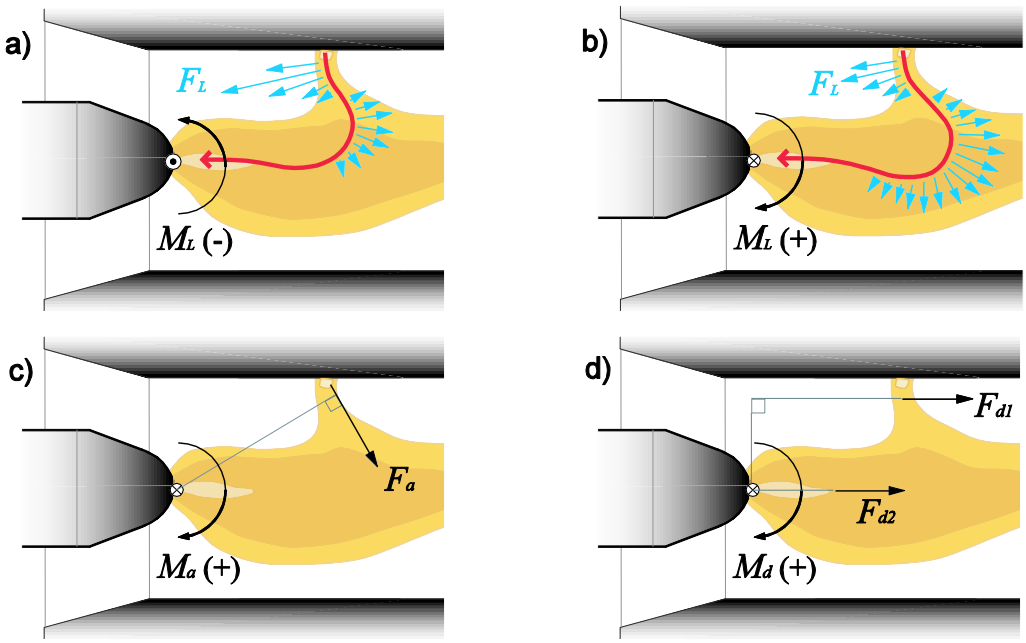

Fig. 10. Forces (F) and angular momentums (M) acting on the arc. a) Lorentz force (F_L) producing a net negative momentum (M_L); b) F_L producing a net positive momentum; c) M_a, angular momentum produced by the anode jet; d) M_d, angular momentum produced by the drag from the interaction cold flow - anode column (F_{d1}) and cold flow - arc column (F_{d2}).

4.3. Voltage Drop Evolution

The reattachment process described in the previous section is repeated in a quasi-periodic form. To observe more clearly the nature of the movement of the arc, Fig. 11 presents the evolution in time of the voltage drop for the cases studied. Each peak corresponds to the establishment of new attachment. It can also be observed that, as the total current increases, so does the reattachment frequency. These results are in qualitative agreement with experimental

findings[2, 3, 4, 5, 6, 7]. The almost unchanged evolution of voltage drop for case 5 (argon, 600 A, 60 slpm) indicates that the torch is operating in steady mode.

Fig. 12 shows the evolution in time and in frequency space of the different characteristics of the arc. It is clear the strong correlation among the different characteristics of the flow, as previously observed experimentally in Refs. 3 to 7. In our simulations, the dominant frequencies are almost 21 kHz, compared to frequencies of ~10 kHz presented in Ref. 6 for the same torch and operating conditions.

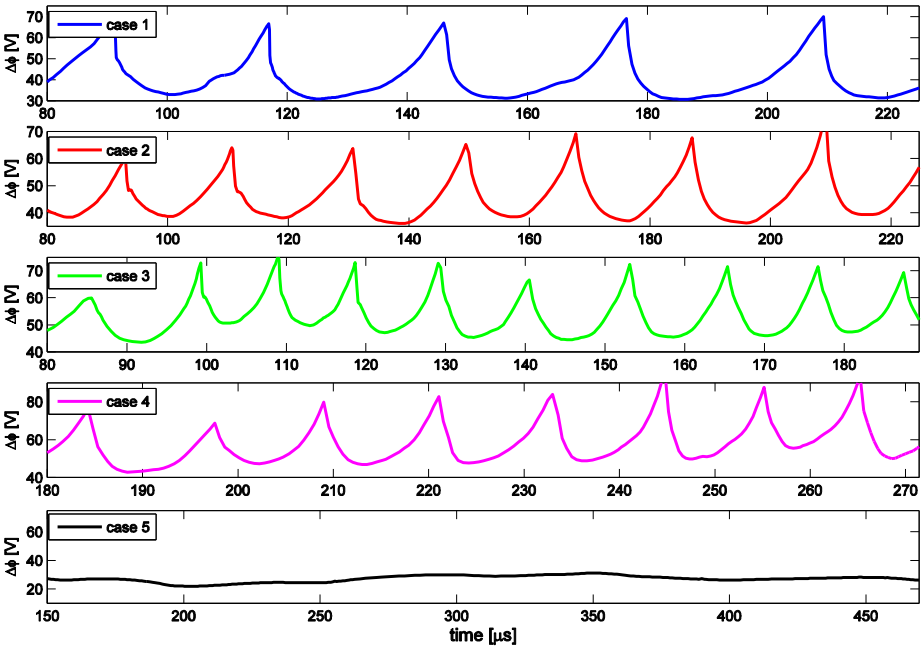

Fig. 11. Time evolution of voltage drop for all cases.

The rapid variation of properties with time is an indication of the "stiffness" of the problem. Stiff problems are characterized by different time scales which make them difficult to simulate. The use of an implicit solver and an adaptive time stepping procedure seems essential to adequately capture the dynamics of the arc.

5. CONCLUSIONS

The dynamics of the arc inside a direct current non-transferred arc plasma torch are simulated using a 3D, transient, LTE mathematical model with a variational multiscale numerical model. Simulations of a torch operating with argon and argon-hydrogen under different operating conditions are presented. The model is able to predict the operation of the torch in steady and takeover modes without any further assumption on the reattachment process except for the use of an artificially high electrical conductivity near the electrodes. This assumption is needed because equilibrium is assumed. The results obtained indicate that the reattachment process in these operating modes may be driven by the movement of the arc rather than by a breakdown-like process. It is also found that, for a torch operating in these modes and using straight gas injection, the arc tends to re-attach to the opposite side of its original attachment. This phenomenon seems to be produced by a net angular momentum on the arc due to three effects: the Lorentz force acting along the arc, the variation of momentum caused by the anode jet, and the drag caused by the interaction between the gas flow and the arc. It is expected that the agreement of the model will diminish as the arc is driven towards the restrike mode of operation due to the possible

dominance of non-equilibrium effects in the reattachment process. From the obtained results, it is clear that a non-equilibrium model is necessary to better describe the dynamics of the arc (avoiding the use of an artificially high electrical conductivity near the electrodes) and its interaction with the electrodes (i.e. heat transfer to the anode). Furthermore, the prescription of better boundary conditions at the outlet (i.e. include part of the jet) and at the anode (i.e. include part of the anode) are expected to provide better results of the dynamics of the arc.

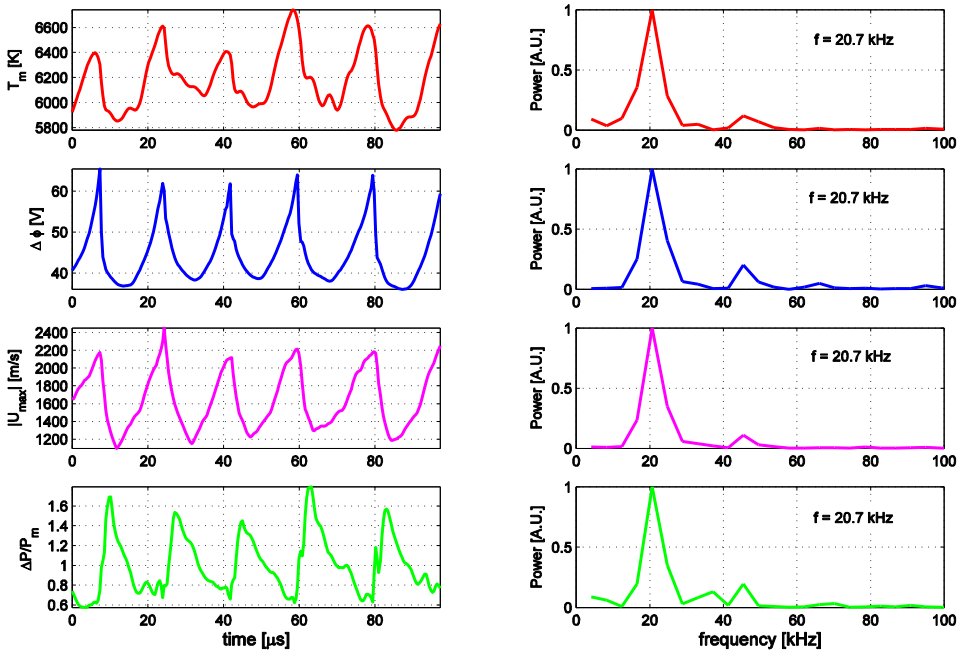

Fig. 12. Time evolution and frequency spectra of mean temperature, voltage drop, maximum velocity, and pressure difference for case 3.

ACKNOWLEDGMENTS

This research has been supported by NSF Grant CTS-0225962. Computing time from a grant from the University of Minnesota Supercomputing Institute is gratefully acknowledged.

REFERENCES

1. P. Fauchais, "Understanding plasma spraying", *J. Phys. D: Appl. Phys.* **37**, R86-108 (2004).
2. S. A. Wutzke, "Conditions governing the symptomatic behavior of an electric arc in a superimposed flow field", *PhD Thesis*, Department of Mechanical Engineering, University of Minnesota (1967).
3. Z. Duan, J. Heberlein, S. Janisson, K. Wittmann, J. F. Coudert and P. Fauchais, "Effects of nozzle fluid dynamics on the dynamic characteristics of a plasma spray torch", *United Thermal Spray Conf.*, *Tagunsgsband Conf. Proc.*, ed. E. Lugscheider and P. A. Kammer (1999).
4. Z. Duan, "Investigations of plasma instabilities in a spray torch", *PhD Thesis*, Department of Mechanical Engineering, University of Minnesota (2000).
5. Z. Duan and J. V. R. Heberlein, "Arc instabilities in a plasma spray torch", *J. of Thermal Spray Technology* **11**, 44-51 (2002).

6. J. F. Coudert and P. Fauchais, "Arc instabilities in a D.C. plasma torch" *High Temp. Material Processes* **1**, 149-166 (1997).
7. J. F. Coudert, M. P. Planche and P. Fauchais, "Characterization of D.C. plasma torch voltage fluctuations", *Plasma Chem. Plasma Proc.* **16**(1), 211s-227s (1996).
8. Li He-Ping and Chen Xi, "Three-dimensional modelling of a DC non-transferred arc plasma torch", *J. Phys. D: Appl. Phys.* **34**, L99-L102 (2001).
9. Li He-Ping, Chen Xi and E. Pfender, "Application of Steenbeck's minimum principle for three-dimensional modeling of DC arc plasma torches", *J. Phys. D: Appl. Phys.* **36**, 1084-1096 (2003).
10. J. J. Gonzales, P. Freton and A. Gleizes, "Comparisons between two- and three-dimensional models: gas injection and arc attachment", *J. Phys. D: Appl. Phys.* **35**, 3181-3191 (2002).
11. L. Klinger, J. B. Vos and K. Appert K, "High-resolution CFD simulation of a plasma torch in 3 dimensions", *Centre de Recherches en Physique des Plasmas - Preprint Report*, LRP 763, http://crppwww.epfl.ch/ (2003).
12. J. M. Park, K. S. Kim, T. H. Hwang and S. H. Hong, "Three-dimensional modeling of arc root rotation by external magnetic field in non-transferred thermal plasma torches", *IEEE Trans. Plasma Sci.* **32**, 479-487 (2004).
13. C. Baudry, A. Vardelle and G. Mariaux, "Numerical modeling of a DC non-transferred plasma torch: movement of the arc anode attachment and resulting anode erosion", *High Tech. Plasma Proc.* **9**, 1-15 (2005).
14. C. Baudry, A. Vardelle, G. Mariaux, C. Delalondre and E. Meillot, "Three-dimensional and time-dependent model of the dynamic behavior of the arc in a plasma spray torch", *Proc. Int. Thermal Spray Conf.* (2004).
15. C. Baudry, "Contribution à la modélisation instationnaire et tridimensionnelle du comportement dynamique de l'arc dans une torche de projection plasma", *Doctoral Thesis*, Universite de Limoges (2003).
16. V. Colombo and E. Ghedini, "Time dependent 3-D simulation of a DC non-transferred arc plasma torch: anode attachment and downstream region effects", *Proc. of the 17th Int. Symp. Plasma Chemistry* (2005).
17. B. E. Launder and D. B. Spalding, *Lectures in mathematical models of turbulence* (New York:Academic) 131-156 (1972).
18. L. Niemeyer and K. Ragaller, "Development of Turbulence by the Interaction of Gas Flow with Plasmas", *Zeitschrift Fur Naturforschung* Band 28a, 1281-1289 (1973).
19. T. J. R. Hughes, "Multiscale phenomena: green's functions, the dirichlet-to-neuman formulation, sub-grid scale models, bubbles and the origins of stabilized methods" *Comput. Methods Appl. Mech. Engrg.* **127**, 387-401 (1995).
20. T. J. R. Hughes, G. R. Feijoo, L. Mazei and J. B. Quincy, "The variational multiscale method - a paradigm for computational mechanics", *Comput. Methods Appl. Mech. Engrg.* **166**, 3-24 (1998).
21. G. Hauke and T. J. R. Hughes "A comparative study of different sets of variables for solving compressible and incompressible flows", *Comput. Methods Appl. Mech. Engrg.* **153**, 1-44 (1998).
22. R. Codina, "On stabilized finite element methods for linear systems of convection-diffusion-reaction equations", *Comput. Methods Appl. Mech. Engrg.* **188**, 61-82 (2000).
23. T. J. R. Hughes, G. Scovazzi and L. Franca, "Multiscale and stabilized methods", *Encyclopedia of Computational Mechanics* vol 3 ed. E. Stein, R. de Borst and T. J. R. Hughes (John Wiley & Sons Inc. USA) (2004).
24. A. Kaddani, S. Zahrai, C. Delalondre and O. Simonin, "Three-dimensional modelling of unsteady high-pressure arcs in argon", *J. Phys. D: Appl. Phys.* **28**, 2294-2305 (1995).
25. G. E. Georghiou, A. P. Papadakis, R. Morrow, and A. C. Metaxas, "Numerical modeling of atmospheric pressure gas discharges leading to plasma production", *J. Phys. D: Appl. Phys.* **38**, R303-R328 (2005).

26. A. B. Murphy, "Demixing in free-burning arcs", *Phys. Rev. E.* **55**, 7473–7494 (1997).
27. E. Pfender, "Plasma: General Computer Code for the Calculation of Thermodynamic and Transport Properties", High Temperature and Plasma Laboratory, Department of Mechanical Engineering, University of Minnesota (1992).
28. X. Zhou and J. Heberlein, "An experimental investigation of factors affecting arc-cathode erosion", *J. Phys. D: Appl. Phys.* **31**, 2577-2590 (2001).
29. T. J. R. Hughes and M. Mallet, "A new finite element formulation for computational fluid dynamics: III the generalized streamline operator for multidimensional advective-diffusive systems", *Comput. Methods Appl. Mech. Engrg.* **58**, 305-328 (1986).
30. T. J. R. Hughes and M. Mallet, "A new finite element formulation for computational fluid dynamics: IV a discontinuity-capturing operator for multidimensional advective-diffusive systems", *Comput. Methods Appl. Mech. Engrg.* **58**, 329-336 (1986).
31. K. E. Jansen, C. H. Whiting and G. M. Hulbert, "A generalized-α method for integrating the filtered navier-stokes equations with a stabilized finite element method", *Comput. Methods Appl. Mech. Engrg.* **190**, 305-319 (2000).
32. V. M. Calo, "Residual-based multiscale turbulence modeling: Finite volume simulations of bypass transition", *PhD Thesis*, Department of Civil and Environmental Engineering, Stanford University (2004).
33. U. Ghia, K. N. Ghia, and C. T. Shin, "High-Re solutions for incompressible flow using the Navier-Stokes equations and a multigrid method", *J. Comp. Phys.* **48**, 387-411 (1982).